SOLO E RECURSOS HÍDRICOS

conservação, recuperação e manejo

ARISTON DA SILVA MELO JÚNIOR
(organizador)

EDITORA ARTEMIS
2022

SOLO E RECURSOS HÍDRICOS

conservação, recuperação e manejo

ARISTON DA SILVA MELO JÚNIOR
(organizador)

EDITORA ARTEMIS
2022

Editora Chefe	Profª Drª Antonella Carvalho de Oliveira
Editora Executiva	M.ª Viviane Carvalho Mocellin
Direção de Arte	M.ª Bruna Bejarano
Diagramação	Elisangela Abreu
Organizador	Prof. Dr. Ariston da Silva Melo Júnior
Imagem da Capa	Ziglinda/123RF
Bibliotecária	Janaina Ramos – CRB-8/9166

Editora Artemis
Curitiba-PR Brasil
www.editoraartemis.com.br
e-mail:publicar@editoraartemis.com.br

Editora Artemis
Curitiba-PR Brasil
www.editoraartemis.com.br
e-mail:publicar@editoraartemis.com.br

Dados Internacionais de Catalogação na Publicação (CIP)

S689 Solo e recursos hídricos: conservação, recuperação e manejo / Organizador Ariston da Silva Melo Júnior. – Curitiba-PR: Artemis, 2022.

Formato: PDF
Requisitos de sistema: Adobe Acrobat Reader
Modo de acesso: World Wide Web
Inclui bibliografia
ISBN 978-65-87396-67-5
DOI 10.37572/EdArt_290822675

1. Solos. 2. Recursos hídricos. 3. Sustentabilidade. I. Melo Júnior, Ariston da Silva (Organizador). II. Título.
CDD 631.45

Elaborado por Bibliotecária Janaina Ramos – CRB-8/9166

EDITORA ARTEMIS
2022

Editora Artemis
Curitiba-PR Brasil
www.editoraartemis.com.br
e-mail:publicar@editoraartemis.com.br

APRESENTAÇÃO

O título **Solo e Recursos Hídricos – Conservação, Recuperação e Manejo** traz para o mundo atual uma das maiores preocupações com a preservação do nosso planeta e dos biomas que compõem toda a estrutura da Terra. O estudo constante de novas tecnologias, metodologias e gerenciamento deve promover um crescimento sustentável e garantir o futuro das próximas gerações.

A importância desse tema nesse século XXI é tamanha que a própria Organização das Nações Unidas (ONU) apresenta em sua agenda de 2030 o tema sustentabilidade e manutenção do meio ambiente como meta de desafio a ser alcançado de forma a que os recursos hídricos e a conservação do solo sejam foco primordial de interesse e responsabilidade politica e social das nações. Tal proposta da ONU já vem sendo empregada por governos em projetos como, por exemplo, cobrança d'água do setor agrícola para minimizar a poluição de rios e lagos e impedir a contaminação de solos. Sendo esse controle realizado pelos denominados Comitês de Bacias Hidrográficas, o que mostra a relevância e atualidade do presente livro.

Este livro não se propõe a trazer soluções finais e vindouras, o que seria pretencioso; mas apresentar a preocupação e zelo que os autores tiveram em compartilhar seus conhecimentos. Assim, o livro apresenta o que de melhor está sendo realizado no mundo acadêmico e cientifico, de modo a trazer propostas, ensaios científicos e reflexões que permeiem as mentes de todos e todas de modo a podermos trazer uma nova proposta de melhoria a manutenção da qualidade e fertilidade de nossos solos e de técnicas para o uso racional das reservas hídricas do mundo, com os novos conceitos que vem sendo estudados pelas universidades e centros de pesquisas em relação ao bioma terrestre e aquático. Exemplos como a chamada pegada hídrica e claro apresentar uma nova proposta pedagógica em que as novas gerações tenham em mente a responsabilidade em um continuo respeito a nosso lar – planeta Terra.

Nesse sentimento que a organização dessa obra propõe uma leitura critica e atenta às pesquisas que os autores e autoras trazem nessa obra de modo a permitirem a generosidade em compartilhar seus conhecimentos e pensamentos para a formação contínua do leitor e leitora.

Uma boa leitura a você leitor/leitora e que as próximas páginas possam levar a uma reflexão da importância sustentável que esse livro tem como meta e sonho: um mundo novo, melhor e mais harmônico para toda humanidade!

Ariston da Silva Melo Júnior

SUMÁRIO

CAPÍTULO 6

FLOW VELOCITY STRUCTURE AND TURBULENCE CHARACTERISTICS IN A PARTIALLY VEGETATED CHANNEL WITH RIGID EMERGENT VEGETATION

Data de submissão: 09/06/2022
Data de aceite: 24/06/2022

Cristina Maria Sena Fael
University of Beira Interior
Centre of Materials and Building Technologies
Department of Civil Engineering and Architecture
Portugal
https://orcid.org/0000-0002-6943-6537

César Augusto Vaz Santos
University of Beira Interior
Centre of Materials and Building Technologies
Department of Civil Engineering and Architecture
Portugal
https://orcid.org/0000-0001-6631-8378

Cátia Sofia Batista Taborda
University of Beira Interior
Centre of Materials and Building Technologies
Department of Civil Engineering and Architecture
Portugal
https://orcid.org/0000-0001-7131-892X

ABSTRACT: Research of hydrodynamics interactions between in-channel vegetation and the main channel is essential for researchers and hydraulic engineers to design, manage and rehabilitate river systems. This chapter intends to experimentally analyse how the hydrodynamic structures of the flow are affected by rigid emergent vegetation occupying a third of the channel width, with a steady flow rate and subcritical conditions. The hydrodynamic flow conditions in the flume are characterised by measurements of instantaneous velocities using 3D Acoustic Doppler Velocimetry, focusing on the obstructed-unobstructed interface area. Overall, the present research demonstrated that the turbulence characteristics are influenced by vegetation density and that these change in the measured depths.
KEYWORDS: Turbulent flow. Vegetated corridor. Experimental study.

1 INTRODUCTION

The presence of vegetation in river systems, on riverbanks or floodplains, under natural conditions or as a result of restoration projects, in addition to contributing to the improvement of their physical characteristics, contributes to the maintenance of ecological standards (Vargas-Luna et al., 2018; Chembolu et al., 2019). Meanwhile, the vegetation can significantly change the flow structure and turbulent characteristics of local and reach-

scale flow, influencing riverine habitat (Crowder and Diplas, 2002), water quality (Devi et al., 2019), dispersion of pollutants and nutrients (Perucca et al., 2009) and transport of sediments (Kothyari et al., 2009).

It is consensual that vegetation in water channels, due to the hydraulic resistance in this area, generates an inflectional profile of the longitudinal velocity in the spanwise direction and a turbulence intensity between the two zones of the channel quite different from those commonly found in non-vegetated flows (e.g., Nepf, 1999). The vegetated corridor induces a reduction in the longitudinal velocity, generating a strong velocity gradient between the two channel areas, creating instability that makes the flow susceptible to the generation of large-scale coherent structures that can significantly influence the pattern and magnitude of turbulence in the local and reach-scale flow turbulence (Yager and Schmeeckle, 2013).

Advances in understanding the turbulent flow characteristics in channels with adjacent vegetated corridors can give design engineers knowledge and tools to improve the design of partially vegetated channels. In recent years, ecological restoration projects have used artificial vegetation as a measure of ecological regulation (Liu et al., 2021). Since this is a central and not yet closed subject, the present work aims to contribute to improving the understanding of the effects of vegetation on the characteristics of the flow and its turbulent structure in partially vegetated channels with rigid and emergent vegetation.

2 EXPERIMENTAL SETUP AND METHODOLOGY

The experimental tests were carried out in the flume located at the Laboratory of Fluvial Hydraulics and Structures of Universidade da Beira Interior, Portugal (Figure 1). The channel, 12.60 m long, 0.80 m wide and 0.70 m deep, has a 0.30 m wide riparian corridor on the right side. Two densities of a staggered matrix of rigid emergent stems were tested, 500 stems.m^{-2} and 1034 stems.m^{-2}, designated in this study as M1 and M2, respectively. This configuration with a quasi-rigid behaviour is a representative range of vegetation densities found in nature (Maji et al., 2020). The water flow is pumped from a downstream reservoir with a capacity of 3.5 m^3 through a pressurized system and an electric pump group. The flow discharge was 104 m^{3}h^{-1}, and it was monitored by an electromagnetic flowmeter, with an error of ± 2%. Downstream of the channel, an adjustable tailgate allowed setting the flow depth, , H at 10 cm. An acceleration ramp and a honeycomb diffuser at the channel inlet smooth the flow trajectories and guarantee uniform crosswise flow distribution.

Measurements of instantaneous 3D flow velocities were performed with a down-looking Acoustic Doppler Velocimeter (ADV), manufactured by Nortek, with a

sampling frequency of 100 Hz and a sampling time of 3 minutes (18000 samples). The three components of velocity, u, v, and w, are the streamwise, spanwise, and vertical velocities in the x, y, and z directions, respectively. The origin of the Cartesian coordinate system is $x = 0$ at the channel inlet and positive in the direction of the flow, $y = 0$ at the vegetation interface and positive towards the left wall (looking downstream), and $z = 0$ at the channel bed and positive upwards. The data was acquired in a section where uniform flow conditions ($x = 8.50$ m) were present in 17 and 20 cross-sectional measurements for matrices M1 and M2. No point was less than 5 cm away from the walls to ensure no wall-related interferences in the measurements. The filter implemented in the WinADV software, as proposed by Goring and Nikora (2002) and modified by Wahl (2003), was used for data processing. The values of the main variables and parameters that characterize the tests for the measuring depths of 0.09 and 0.39 are summarized in Table 1.

Table 1 – Characteristic experimental parameters for both test runs.

Tests	z/H [-]	ϕ [-]	U_1 [ms^{-1}]	U_2 [ms^{-1}]	U_c [ms^{-1}]	ΔU [ms^{-1}]	λ [-]	δ [m]	θ [m]	$C_D a$ [ms^{-1}]
M1	0.09	0.039	0.071	0.462	0.267	0.391	0.732	0.190	0.039	3.11
	0.39	0.039	0.071	0.553	0.312	0.482	0.773	0.196	0.039	3.19
M2	0.09	0.081	0.050	0.455	0.253	0.405	0.802	0.143	0.035	8.76
	0.39	0.081	0.046	0.567	0.306	0.521	0.851	0.106	0.035	10.52

In Table 1, the equilibrium velocity in the inner part of the vegetated area and the peak velocity in the main channel are U_1 and U_2, respectively; the solid volume fraction is $\phi = \pi d^2 N/4$, where d is the stem diameter and N is the number of stems per unit area; the mean longitudinal velocity is $U_c = (U_1 + U_2)/2$; the velocity differential is $\Delta U = U_2 - U_1$; the velocity ratio $\lambda = \Delta U/U_c$; the mixing layer thickness is δ , estimated as suggested by White and Nepf (2007) employing the definition of the hyperbolic tangent profile and a boundary layer analogy; the momentum thickness is $\theta = \int_{-\infty}^{+\infty} \left[1/4 - \left((U(y) - U_c)/\Delta U\right)^2\right]$; and $C_D\, a$ is the drag density parameter, where $a = Nd$ is the frontal projected area per unit volume and C_D is the drag coefficient for the vegetation array and was estimated through $C_D\, aU_1^2\, /2 = -gdH/dx$, where g is the acceleration of gravity, neglecting the contribution of turbulent and dispersive stresses and assuming equilibrium between the drag force and the imbalance between hydrostatic pressure forces between two arbitrary cross-sections, as suggested by White and Nepf (2007).

Figure 1 – Schematics of the experimental setup: a) longitudinal view; b) stem density and measurement points; c) depth range.

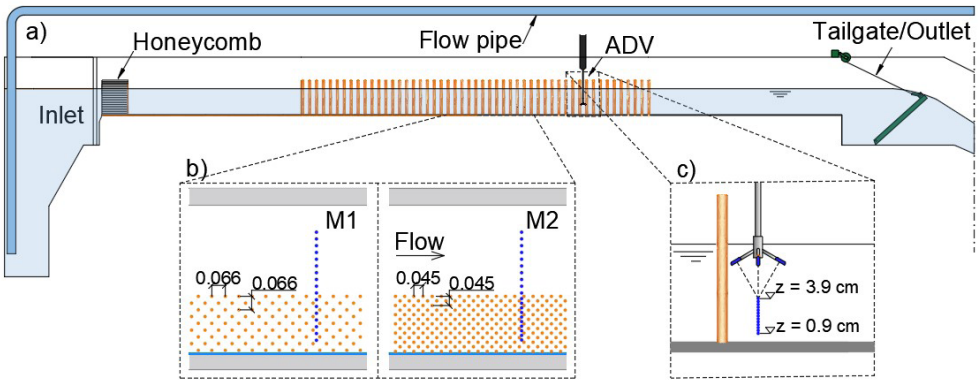

In this manuscript, the flow properties addressed, in addition to being investigated near the bottom $z/H=$ 0.09, were also analysed approximately at mid-depth ($z/H=$ 0.39), as these depth measurements were within 5% of the depth-averaged velocity. This criterion has already been used in previous investigations, e.g., White and Nepf (2007) and Caroppi (2018).

3. RESULTS AND DISCUSSION

3.1 MEAN FLOW

In a turbulent flow, each velocity component has the characteristics of a rapidly varying random function of time and space for a given measurement point. Given the complexity of turbulent flows, Reynolds decomposition is applied to the Navier-Stokes equations, which separates the instantaneous value of the flow variables into their time-averaged values and respective fluctuations. For example, applying this concept to the streamwise velocity results in $u_i=u+u'$, where u_i, u, and u' are, respectively, the instantaneous, mean, and fluctuating velocities. As a result of the Reynolds decomposition, statistical concepts characterise the flow. Therefore, the time-averaged velocity in the streamwise direction is given by $u = 1/n \sum_{i=1}^{n} u_i$, where n is the number of samples. The same procedure can be applied to the three flow directions.

Figure 2 shows the lateral distribution of u velocities for the experimental series M1 and M2, at $z/H=$ 0.09 and 0.39. In the figure, the dashed line represents the interface between the vegetation and free regions. For both matrices and measuring depths under analysis, the longitudinal velocity becomes constant within the vegetation, U_1 and at the centre of the main channel, U_2. In the main channel, u at mid-depth is 18% and 11% higher

than the velocities near the bottom for M1 and M2, respectively. The figure also shows that the velocity gradient increases with the vegetation density, consequently decreasing the penetration of the mixing layer. A smaller spanwise gradient of the longitudinal velocity is observed for the profiles near the bottom and therefore there is a higher penetration of the shear layer into the vegetation (Table 1).

Figure 2 – Lateral distribution of the streamwise velocity: a) matrix M1; b) matrix M2.

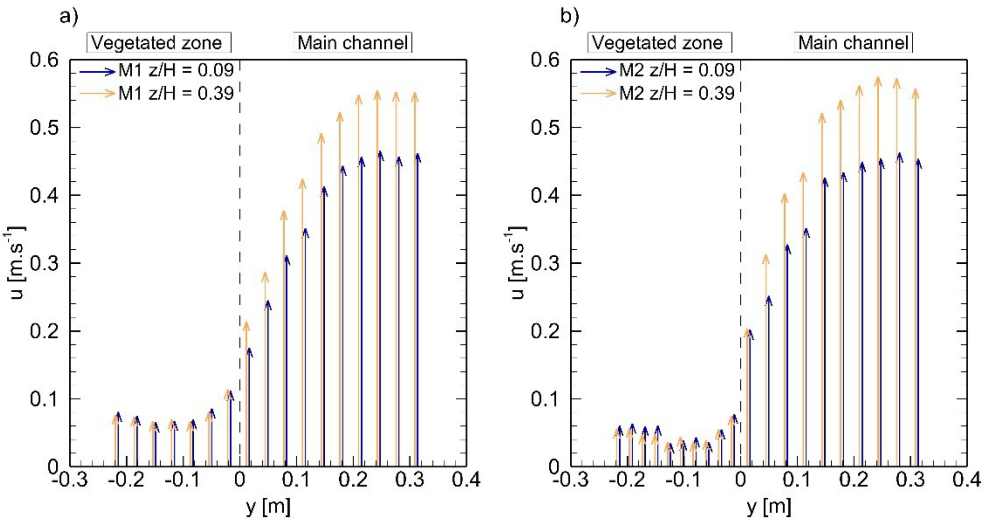

Figure 3 depicts the distribution of the velocity vectors of the secondary currents v–w, up to the mid-depth of the flow, for the two vegetation density matrices. In the innermost part of the vegetation, the dominant flow that is observed is the flow around each stem. However, if the local effect of the stems is discounted, that is, the flow on the left and right sides of the stem, there is a well-defined trend of net flow towards the open central channel. This trend gains intensity and accelerates the flow towards the main central channel. It can be observed that the highest transport of mass and momentum towards the central channel by the secondary current occurs near the bottom, where the component v of the velocity vector is of great intensity. At the interface, on the side of the central channel, the intensity of the secondary current decreases with increasing vegetation density.

Figure 3 – Velocity vectors in the y - z plane, for M1 and M2.

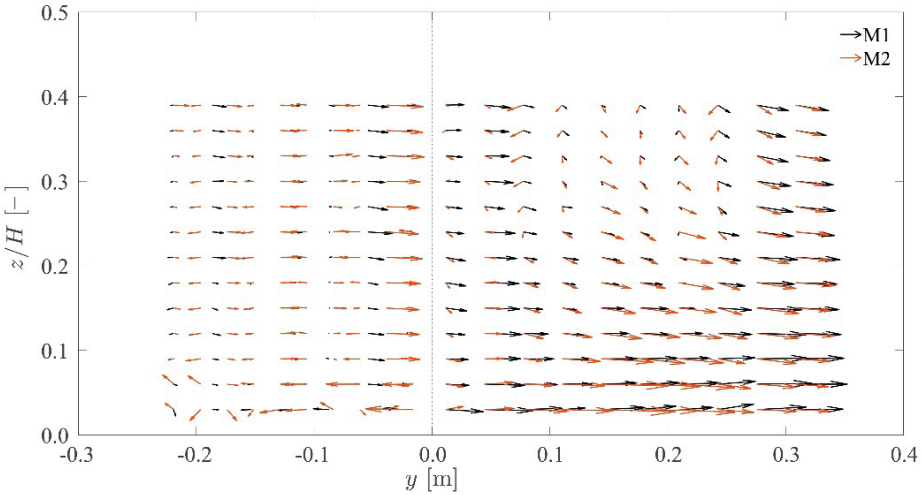

3.2 TURBULENCE INTENSITY, REYNOLDS SHEAR STRESS AND TURBULENCE KINETIC ENERGY

The Navier-Stokes equations are the governing equations of fluid dynamics and can describe the velocity fields of turbulent flow, from the largest to the smallest turbulent scale. Given their complexity, the Reynolds decomposition is applied to the continuity and momentum equations. It is, precisely, from the convective terms of the momentum equations that the Reynolds stress tensor, $-\rho\overline{u_i' u_j'}$, arises. This new term represents the stresses induced in the flow field by turbulent effects. The diagonal components of the tensor are the normal stresses, and the off-diagonal ones are the shear stresses.

The turbulence intensities in the streamwise, spanwise and vertical directions (σ_u, σ_v and σ_w) were evaluated as the root-mean-square of the fluctuating velocity. For instance, for the streamwise turbulence intensity, $\sigma_u = \sqrt{\left(1/n \sum_{i=1}^{n} {u_i'}^2\right)}$. The turbulence intensity, resulting from the variation of the instantaneous velocity at a given measurement point, reflects the number of fluctuations in the turbulent field, providing information regarding the contribution of these fluctuations to the production of flow turbulence (Caroppi, 2018, Devi et al., 2016). The Reynolds shear stress can be calculated through the covariance of the fluctuating velocity, $\tau_{uv} = -\rho COV_{uv} = -\rho/n \sum_{i=1}^{n} u_i' v_i'$, where ρ is the water density. This shear stress reflects the turbulent fluctuations in the flow field, giving helpful information on the momentum transfer. From the trace of the Reynolds stress tensor, it is possible to determine the total turbulent intensity, which can describe the turbulent flow structure, designated the turbulence kinetic energy (TKE) and is defined as $K = 0.5(\sigma_u^2 + \sigma_v^2 + \sigma_w^2)$.

The lateral profile of streamwise and spanwise turbulence intensities, σ_u and σ_v, are presented in Figure 4. A similar trend for both matrices can be observed in Figure 4a: a peak at the interface on the side of the central channel when $z/H=$ 0.39 and shifted towards the centre of the main channel when $z/H=$0.09. The spanwise gradients are higher on the vegetation side, decreasing successively into the innermost part of the vegetation, and the turbulence intensity in the vegetation corridor is lower than in the main channel. Additionally, the gradient in the spanwise direction of σ_u near the bottom is less pronounced than at mid-depth. In all cases, turbulence intensities are higher for the matrix with the highest density, M2. At the interface, σ_u is approximately 30% higher at mid-depth than near the bottom, and in the middle of the channel, this trend is reversed, and σ_u is higher near the bottom. Furthermore, as already observed by Nezu and Onitsuka (2001) for partially vegetated channels with submerged vegetation, Figure 4b shows that the peak of σ_v, for both flow depths, is slightly shifted towards the main channel, whereby in the main channel, the lateral turbulent intensity is on average 35% higher near the bottom than at mid-depth.

Figure 4 – Lateral distribution of turbulence intensities: a) streamwise; b) spanwise.

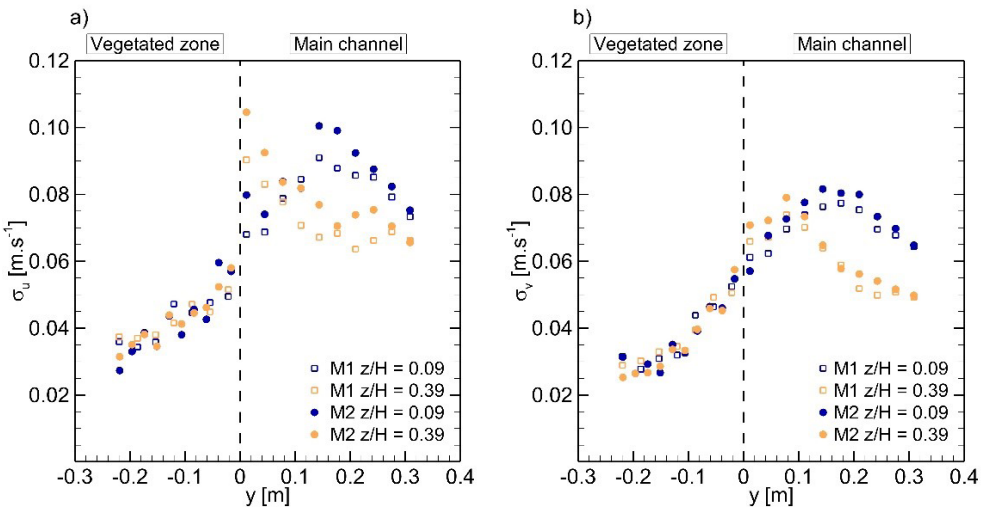

The Reynolds shear stress, τ_{uv}, for $z/H=$ 0.09 and $z/H=$ 0.39 are presented in Figure 5a along the transversal section for M1 and M2. From the spanwise distribution, τ_{uv} at mid-depth is, on average, three times higher than near the bottom at the interface between the vegetated corridor and the central channel. The results are intelligible since these stresses are generated by the instability of the inflectional profile of the velocity in this area, and at mid-depth, as already observed in Figure 2, the streamwise velocity exhibit a higher gradient. The lower values of τ_{uv} near the bottom evidence the

bed resistance to the flow, and it can be concluded that at this height, there is a smaller contribution of momentum transfers by velocity fluctuations to the mean flow, where the horizontal momentum has been absorbed by the vegetation elements regardless of density. Within the vegetation, τ_{uv} assumes values close to zero, regardless of the density of the vegetation or the measuring depth under analysis.

As shown in Figure 5b, withing the vegetation, the turbulence kinetic energy (TKE) displays similar behaviour for both matrices, with increasing values toward the interface and little differences between values at $z/H=$ 0.09 and $z/H=$ 0.39. In the main channel region, however, the behaviour varies with both the water depth and vegetation density, although some similarity remains. For both matrices, the peak of TKE occurs at the vegetation interface for $z/H=$ 0.39, whereas for $z/H=$ 0.09, the peak is located further into the main channel. At the interface, TKE at $z/H=$ 0.39 is 50% higher than near the bed for M1 and 65% higher for M2. According to Caroppi (2018), the vegetation contributes to the dissipation of turbulence larger than the vegetation length scale while also generating turbulence at scales smaller than the vegetation. Given that the interface is a highly unstable region, the velocity fluctuations result in the formation of eddies, enhancing flow turbulence. The smaller values of TKE at $z/H=$ 0.09 can be explained by a higher dissipation of turbulence from both the vegetation and the presence of a boundary (channel bed). This general displacement between the near-bed and mid-d6epth regions can be associated with the higher spanwise transport rate (higher transversal velocities) at $z/H=$ 0.09, as seen in Figure 3. Note how spanwise velocities do not show significant changes as we move away from the peak location of v. However, turbulence parameters (turbulence intensities, Reynolds shear stresses and TKE) start to decrease.

Figure 5 – Spanwise distribution of: a) Reynolds shear stress; b) turbulence kinetic energy.

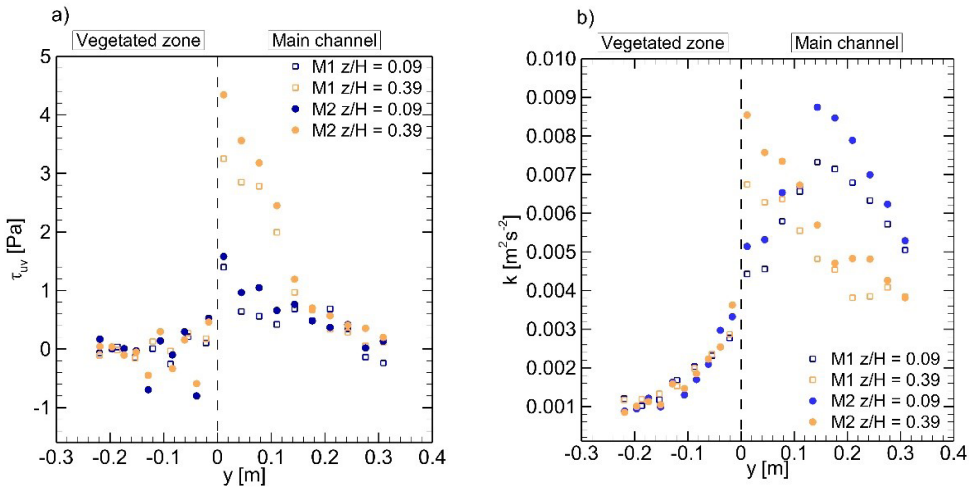

Furthermore, despite the higher streamwise velocities at $z/H=$ 0.39, the flow is, generally, less turbulent than when compared to the near-bed region, as expected, and the turbulence parameters start decaying as soon as we move away from the vegetation interface. At $z/H=$ 0.09, an initial increase is seen, up to the peak value, and only then starts decreasing.

3.3 TURBULENCE SPECTRA

Before undertaking the turbulence spectra, the energy cascade concept (Richardson, 1922) must be introduced. Due to their unstable nature, large eddies break up and transfer their energy onto smaller eddies. This process is repeated until the eddy reaches such a scale that the kinetic energy can be effectively dissipated by the molecular viscosity. In this scope, Kolmogorov (1991) proposed a theory based on two similar hypotheses: in any turbulent flow with high enough Re, the properties of the small-scale motions are entirely dependent on the kinematic viscosity and the dissipation rate ε; there is an intermediate range (inertial subrange) within the small-scale region where the properties of the turbulent motion are determined exclusively by the rate of dissipation ε. These hypotheses show that in the inertial subrange, the energy spectrum is given by $E(k)=C\,\epsilon^{2/3}k^{-5/3}$, where k is the wavenumber and $C=$ 1.5 is a universal constant. The previous equation is the well-known Kolmogorov -5/3 spectrum. Note that during the breakdown process, memory and directionality of the eddies are progressively lost, such that when they reach the Kolmogorov scales, they are, essentially, isotropic. Given that the Reynolds number based on the Kolmogorov scales is equal to 1, it can be inferred that there is a dynamic equilibrium such that the energy dissipated at a rate ϵ, is equal to the rate at which energy is transferred from the larger eddies (Pope, 2000).

The analysis of the turbulence power spectra can provide helpful information on the flow characteristics, as it shows how kinetic energy is distributed as a function of frequency (Caroppi, 2018). Given that the spectrum is one-dimensional, it can present greater insight into the contribution of a given fluctuating velocity component to the turbulent kinetic energy. By aggregating the information of each velocity spectrum, it is possible to generate the spectrogram (Figures 6 and 7) of the velocity fluctuation in the corresponding direction. These figures show that the high energy zones have a greater spanwise extension for $z/H=$ 0.09 than for $z/H=$ 0.39 and are located away from the vegetation interface. Furthermore, the energy is contained in a narrower window of Strouhal number for denser vegetation, which indicates that the energy spectrum decays faster for M2 than it does for M1. According to Figure 5b, peak values of TKE for $z/H=$0.39 occur at the interface, yet according to Figures 6 and 7, the highest energy values are

located further into the main channel. This is a result of the weight of each component to the overall TKE. The spectrogram of the streamwise velocity fluctuation (see Taborda et al. 2022) shows higher energy concentrations near the interface. As such, at this location, the longitudinal component of the velocity is more preponderant to the TKE. As we move away from the vegetation, the longitudinal component loses expression, and the spanwise component takes on higher values, translating into a greater weight of the spanwise component to the overall TKE in this region. Inside the vegetation, the longitudinal and spanwise components have similar weights on the TKE. Finally, note how peak contour values occur for Strouhal closer to the characteristic frequency of Kelvin-Helmholtz vortices (St= 0.032, horizontal dashed line) for the denser vegetation. These coherent structures significantly enhance the lateral mass and momentum transport across the mixing layer (Taborda et al, 2022).

Figure 6 – Spectrogram of the fluctuating spanwise velocity for matrix M1: a) z/H=0.09; b) z/H=0.39.

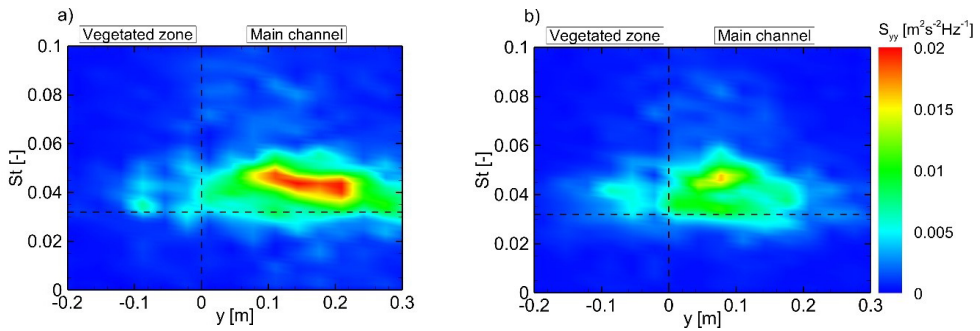

Figure 7 – Spectrogram of the fluctuating spanwise velocity for matrix M2: a) z/H=0.09; b) z/H=0.39.

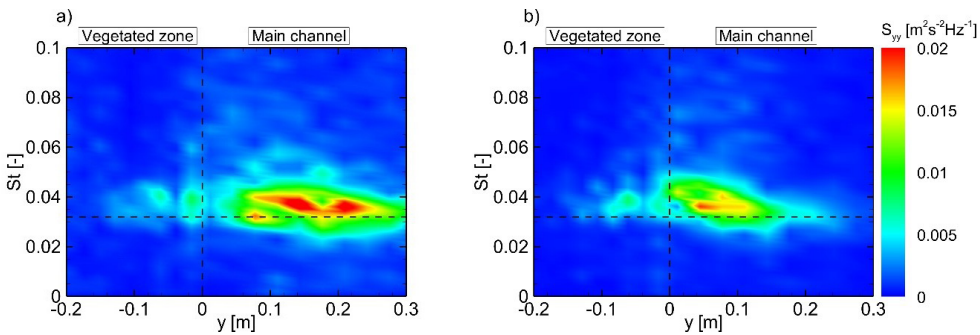

3.4 TURBULENCE ANISOTROPY

Following the previous considerations about the Reynolds stress tensor, a differentiation can be made between the isotropic and anisotropic stresses. The isotropic

part is $2/3K\delta_{ij}$, and the anisotropic part is $a_{ij} = \overline{u_i'u_j'} - 2/3K\delta_{ij}$, where δ_{ij} is the Kronecker delta. The normalization of the anisotropy tensor results in $b_{ij} = \overline{u_i'u_j'}/(2K) - 1/3\delta_{ij}$. The analysis of this tensor can provide valuable information on the amount and type of anisotropy present in the flow. For the visualization of the flow's anisotropy, the current work resorts to the anisotropy invariant map (Choi and Lumley, 2001). The commonly named turbulence triangle is a domain based on the second, II, and third, III, invariants of the normalized anisotropy tensor. The borders of the triangle correspond to special states of turbulence, and according to Lumley (1978), all possible states of turbulence must occur within the triangle. Thus, the ensuing invariant maps, in the ξ–η coordinate, are depicted in Figure 8, where $\xi = \sqrt[3]{III/2}$ and $\eta = \sqrt[2]{-II/3}$.

Figure 8 – Invariant maps for a) M1 and b) M2. Blue markers are for z/H= 0.09, and orange markers for z/H= 0.39. Square, circle and triangle markers represent, respectively, values for the vegetation zone, interface and main channel.

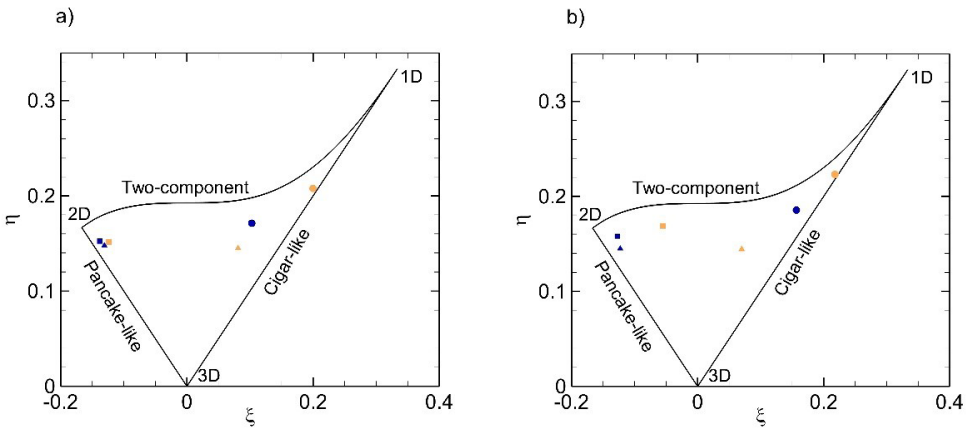

From Figure 8, it can be seen that the turbulence has a high degree of anisotropy, given that all the points are close to the triangle's upper boundary, regardless of vegetation density and measurement location. At the vegetation interface, however, turbulence anisotropy is predominantly 1D, where one component of the TKE is greater than the other two. Additionally, this effect is exacerbated at the mid-depth, seeing that the points are closer to the right boundary and closer to the 1D vertex. Inside the vegetation, the flow is characterised by 2D axisymmetric turbulence, where two components of the TKE are greater than the other one.

4 CONCLUSIONS

In the present research, a laboratory study was conducted to analyse the flow characteristics in a channel partially covered by a finite length of staggered matrices of

vertical, cylindrical, rigid, and emergent stems. The results showed that the longitudinal velocity gradient increases with vegetation density, leading to a decrease in the penetration of the mixing layer into the vegetation. In the depth comparison, the lowest longitudinal velocity gradient is observed for profiles close to the bottom, presenting greater penetration of the shear layer within the vegetation. For this kind of free-surface turbulent flow, the secondary currents are one of its intrinsic characteristics. In this study it was verified that the most significant transport of mass and momentum towards the central channel occurs near the bottom. As a result of the instability of the inflectional velocity profile, Reynolds shear stresses are generated, presenting lower values near the bottom, which denotes the effects of the bed's resistance to flow. It was also shown that the Reynolds shear stresses assume values close to zero within the vegetation, regardless of the vegetation density or the analysed measurement depth. The present research demonstrated that the turbulence kinetic energy within the vegetation presents similar behaviours for both matrices, increasing values towards the interface and minor variations in depth. The lower values of turbulence kinetic energy near the bottom can result from the greater dissipation of turbulence caused by vegetation and the channel bed.

5 ACKNOWLEDGEMENTS

The authors would like to thank for the financial support of the Portuguese Foundation for Science and Technology (FCT) through Project PTDC / ECI-EGS / 29835/2017 - POCI-01-0145-FEDER-029835, financed by FEDER funds through COMPETE2020 - Operational Program Competitiveness and Internationalization (POCI) and by National funds through FCT, and for the Portuguese national funds by FCT within the C-MADE UIDB/04082/2020.

REFERENCES

Caroppi, G. (2018). **Turbulence in partly vegetated channels: Experiments with complex morphology vegetation and rigid cylinders**. PhD Thesis. Department of Civil, Construction and Environmental Engineering, University of Naples Federico II, Italy.

Chembolu, V., Kakati, R., Dutta, S. (2019). **A laboratory study of flow characteristics in natural heterogeneous vegetation patches under submerged conditions**. Advances in Water Resources. 133, 103418.

Choi, K., Lumley, J. (2001). **The return to isotropy of homogeneous turbulence**. Journal of Fluid Mechanics. 436, 59-84.

Crowder, D.W., Diplas, P. (2002). **Vorticity and circulation: spatial metrics for evaluating flow complexity in stream habitats**. Canadian Journal of Fisheries and Aquatic Sciences. 59 (4), 633-645.

Devi, T.B, Kumar, B. (2016). **Channel Hydrodynamics of Submerged, Flexible Vegetation with Seepage**. Journal of Hydraulic Engineering. 142 (11), 04016053.

Devi, T.B., Sharma, A., Kumar, B. (2019). **Flow characteristics in a partly vegetated channel with emergent vegetation and seepage**. Ecohydrology & Hydrobiology. 19(1), 39-109.

Goring, D.G., Nikora V.I. (2002). **Despiking acoustic doppler velocimeter data**. Journal of Hydraulic Engineering.128:117–126.

Kolmogorov, A. N. (1991). ***The Local Structure of Turbulence in Incompressible Viscous Fluid for Very Large Reynolds Numbers***. Proceedings of the Royal Society A: Mathematical, Physical and Engineering Sciences. 434(1890), 9–13.

Kothyari, U.C., Hayashi, K., Hashimoto, H. (2009). **Drag coefficient of unsubmerged rigid vegetation stems in open channel flows**, Journal of Hydraulic Research. 47:6, 691-699.

Liu, M., Wenxin Huai, W., Ji, B. (2021). **Characteristics of the flow structures through and around a submerged canopy patch**. Physics of Fluids. 33, 035144.

Lumley, J. L. (1978). **Computational modeling of turbulent flows.** Advances in Applied Mechanics. 18, 123-176.

Maji, S., Hanmaiahgari, P.R., Balachandar, R., Pu, J.H., Ricardo, A.M., Ferreira, R.M. (2020). **A Review on Hydrodynamics of Free Surface Flows in Emergent Vegetated Channels**. Water 2020. 12:1218.

Nepf, H. (1999). **Drag, turbulence, and diffusion in flow through emergent vegetation**. Water Resources Research. 35 (2), 479–489.

Nezu, I., Onitsuka, K. (2001). **Turbulent structures in partly vegetated open-channel flows with LDA and PIV measurements**. Journal of Hydraulic Research. 39:629–642.

Perucca, E., Camporeale, C., Ridolfi, L. (2009). **Estimation of the dispersion coefficient in rivers with riparian vegetation**. Advances in Water Resources. 32 (1), 78–87.

Pope, S. (2000). **Turbulent Flows**. Cambridge: Cambridge University Press.

Richardson, L. F. (1922). ***Weather Prediction by Numerical Process.*** Cambridge: Cambridge University Press.

Taborda, C., Fael, C., Ricardo, A., Ferreira, R. (2022). **Wave-like motion and secondary currents in arrays of emergent cylinders induced by large scale eddying motion**. Environmental Fluid Mechanics. 22, 403–428.

Vargas-Luna, A., Crosato, A., Anders, N., Hoitink, A., Keesstra, S., Uijttewaal, W. (2018). **Morphodynamic effects of riparian vegetation growth after stream restoration**. Earth Surf. Process. Landforms. 43: 1591– 1607.

Wahl, T.L. (2003). **Discussion of Despiking acoustic doppler velocimeter data by Derek G. Goring and Vladimir I. Nikora**. Journal of Hydraulic Engineering. 129:487-488.

White, B., Nepf, H. (2007). **Shear instability and coherent structures in shallow flow adjacent to a porous layer**. Journal of Fluid Mechanics. 593:1-32.

Yager, E.M., Schmeeckle, M.W. (2013). **The influence of vegetation on turbulence and bed load transport**. Journal of Geophysical Research: Earth Surface. 118, 1585-1601.

SOBRE O ORGANIZADOR

ARISTON DA SILVA MELO JÚNIOR - GRADUADO em Engenharia agrícola e civil pela Universidade Estadual de Campinas - UNICAMP; com PÓS-DOUTORADO no estudo de sinterização e obtenção de compósitos de terras raras em células à combustível pelo Centro de Ciências de Tecnologia de Materiais (CCTM) e PÓS-DOUTORADO no estudo da poluição atmosférica e a contribuição dos gases de efeito estufa (GEE) no impacto ambiental pelo Centro de Química e Meio Ambiente (CQMA) ambos realizados no Instituto de Pesquisas Energéticas e Nucleares (IPEN) da Universidade de São Paulo - USP. MESTRE em Engenharia de Recursos Hídricos - Água e Solos no estudo da relação e interferência dos parâmetros ecofisiológicos de macrófitas na depuração de esgoto doméstico na Faculdade de Engenharia Agrícola (FEAGRI) da UNICAMP. DOUTOR em Engenharia de Recursos Hídricos e Energéticos estudando a relação e presença de metais pesados dispersos na atmosfera através da coleta de material particulado PM10 e analise pelas técnicas de reflexão total por raios X e microfluorescência com uso de radiação síncrotron aplicadas às analises pela Faculdade de Engenharia Civil, Arquitetura e Urbanismo (FEC) da UNICAMP. Possui mais de 45 artigos publicados com temática no uso da engenharia e tecnológicas de ponta e alternativas para estudo dos processos de tratamentos de resíduos líquidos, gasosos e sólidos. Autor de 5 livros técnicos e de 2 capítulos de livros na área de engenharia civil e sanitária. Membro da Associação de Engenheiros da SABESP (Companhia de Saneamento Básico de São Paulo) atuou como avaliador e examinador na IBFCRL para concursos públicos na área de engenharia civil e agronomia, além de participar em bancas de mestrado e de concursos na UNICAMP e no IFSP. Adepto do ensino continuado realizou mais de 102 cursos de aperfeiçoamento no ensino superior pela Universidade Federal do Ceará, pela Universidade Estadual do Maranhão e outras IES. Possui mais de 10 anos no ensino superior na Universidade Paulista (UNIP); Faculdades Metropolitanas Unidas (FMU); Universidade Braz Cubas e FATEC-SP. Sendo professor nos cursos de Engenharia: Civil; Sanitária e Ambiental; Elétrica; Mecânica; além dos cursos de tecnologia de edifícios; gestão ambiental e arquitetura e urbanismo. Foi coordenador geral do curso de engenharia civil na FMU durante a gestão de 2015-2016. Tem como linha de pesquisa o estudo continuo de novas tecnologias de tratamento de resíduos sólidos e líquidos para depuração e conservação do meio ambiente, atuando como pesquisador colaborador na USP e UNICAMP.

Endereço para acessar este CV: http://lattes.cnpq.br/0010807076892082

ÍNDICE REMISSIVO

R

S

T

V